RNA binding of T-cell intracellular antigen-1 (TIA-1) C-terminal RNA recognition motif is modified by pH conditions*

Isabel Cruz-Gallardo[1], Ángeles Aroca[1], Cecilia Persson[2], B. Göran Karlsson[2] and Irene Díaz-Moreno[1*]

[1]From the Instituto de Bioquímica Vegetal y Fotosíntesis (IBVF), cicCartuja, Universidad de Sevilla-CSIC, Avda. Américo Vespucio 49, Sevilla 41092, Spain.
[2]Swedish NMR Centre, University of Gothenburg, PO Box 465, SE-40530 Gothenburg, Sweden.

*Running title: *pH-dependent RNA binding of TIA-1 RRM3*

To whom the correspondence should be addressed: Dr. Irene Díaz Moreno. Instituto de Bioquímica Vegetal y Fotosíntesis (IBVF), cicCartuja, Universidad de Sevilla-CSIC, Avda. Américo Vespucio 49, Sevilla 41092, Spain. Tel.: 34-954489513; Fax: 34-954460065; E-mail: idiazmoreno@us.es.

Keywords: DNA/RNA binding protein (D/RBP); pH-dependence; NMR; RNA recognition motif (RRM); T-cell intracellular antigen-1 (TIA-1).

Background: T-cell intracellular antigen-1(TIA-1) is a key DNA/RNA binding protein in RNA metabolism.
Results: The binding of TIA-1 RRM3 domain (isolated or fused to RRM2) to RNA is affected by pH changes.
Conclusion: The pH-dependence of RRM3/RNA interaction may have a significant effect in the overall TIA-1 function.
Significance: Unveiling the auxiliary role of RRM3 in RNA recognition sheds light on the TIA-1 function between cell compartments.

SUMMARY

T-cell intracellular antigen-1 (TIA-1) is a DNA/RNA binding protein that regulates critical events in cell physiology by the regulation of pre-mRNA splicing and mRNA translation. TIA-1 is constituted by three RNA recognition motifs (RRMs) and a glutamine rich domain and binds to uridine-rich RNA sequences through its C-terminal domains RRM2 and RRM3. Here we show that RNA binding mediated by either isolated RRM3 or the RRM23 construct is controlled by slight environmental pH changes due to the protonation / deprotonation of TIA-1 RRM3 histidine residues. The auxiliary role of the C-terminal RRM3 domain in TIA-1 RNA recognition is poorly understood and this work provides an insight into its binding mechanisms.

Human T-cell intracellular antigen-1 (TIA-1)[3] is a 46-kDa DNA/RNA binding protein (D/RBP) with a dual regulatory role at the level of transcriptional and post-transcriptional processes shuttling between the nucleus and the cytoplasm (1,2). In the nucleus, TIA-1 regulates the alternative splicing of pre-mRNA (3-5) and modulates gene transcription by binding to DNA (6). In the cytoplasm, TIA-1 regulates the turnover of several mRNAs (7-9) by repressing their translation. To fulfill this function, TIA-1 binds to 3' untranslated regions (UTR's) that are frequently adenine/uridine rich elements (AREs). In addition, recent studies (10) have identified 5' terminal oligopyrimidine tracts (5'TOP) mRNAs – defined as 4-to-15-nucleotide CU-rich elements in 5' UTR's (11,12) – as novel targets for TIA-1/TIAR (TIA-1 related) proteins. Under stress conditions, eIF2α is phosphorylated so the

initiation of translation is inhibited and TIA-1 recruits and escorts noncanonical preinitiation complexes to stress granules (1,13,14).

TIA-1 consists of three RNA recognition motifs (RRM1-3) along with a C-terminal glutamine-rich prion-related domain (PRD) (Figure 1A). Both PRD and the N terminal RRM (RRM1) are involved in U1snRNP recruitment to regulated splice sites (4). Isolated RRM1 binds to single-stranded DNA molecules (ssDNA) (6) but not to RNA (15). However, recent reports show that RRM1 presence enhances TIA-1 affinity for certain RNA sequences (16). RRM2 is necessary for TIA-1 binding to RNAs containing U-rich motifs, whereas RRM3 binds weakly but contributes to improve such binding (15,16).

All TIA-1 RRMs display the canonical αβ fold with the consensus ribonucleoprotein (RNP1 and RNP2) residues for RNA binding (17,18). RRM3 exhibits a non-canonical N-terminal α-helix in a homology model (19) that is conserved in TIAR (PDB ID 1X4G) and Pub1p – the analogous protein in *Sacharomyces cerevisiae* – (20). Moreover, the C-terminal motif Trp-Gly-[Arg/Lys] is also conserved and the β-sheet is slightly distorted (Figure 1B and 1C). Due to their common features, TIA-1/TIAR/Pub1p RRM3 domains are considered a new type of RRM family called TIA-1 C-terminal domain like RRM (TRRM) (19,20). The contribution of RRM3 to RNA recognition is still unclear, although it has been reported its contribution in binding poli-U sequences (16), as well as its role in specifically selecting transcripts (20).

Given the pleiotropic role of human TIA-1 in the control of critical cellular events, understanding how RNA recognition occurs, along with the biophysical features associated, has a great relevance. This work suggests that the auxiliary role in RNA recognition of isolated RRM3 or RRM3 in the RRM23 context is modulated by slight environmental changes in terms of pH, as small changes in protonation / deprotonation of conserved RRM3 histidine residues induce drastic effects over TIA-1 binding to RNA.

EXPERIMENTAL PROCEDURES

Protein and RNA Oligonucleotides Preparation – RRM2 domain (residues 80-173), RRM3 domain (residues 190-288) and RRM23 construct (residues 80-288) were obtained by PCR from the plasmid containing full-length TIA-1 kindly provided by Prof. P. Anderson (Harvard Medical School, USA) and cloned into pETM-11 vector (Invitrogen) as previously described (19). Isotopically ^{15}N and ^{13}C-labeled proteins were expressed in *Escherichia coli* BL21 (DE3) cells in minimal medium (M9) supplemented either with $^{15}NH_4Cl$ or $^{15}NH_4Cl$ and ^{13}C-glucose following the same protocol as in Aroca *et al.*(19) for LB medium. His-tagged TIA-1 constructs were purified by nickel affinity chromatography (Ni Sepharose 6 Fast Flow, GE Healthcare). The His-tag, along the TEV cleavage site, was kept at the constructs since no differences on the secondary structure with or without His-tag were observed (19). Samples were concentrated up to 1 mM in 20 mM potassium phosphate buffer, 50 mM KCl (pH 7.0). Protein concentration was determined by spectrophotometry with predicted extinction coefficients.

RNA 5'AUUUA 3' and 5'AUUUAUUUAUUUAUUUAUUUAUUU 3' oligos were chemically synthesized (IDT, Integrated DNA Technologies).

Nuclear Magnetic Resonance Spectroscopy (NMR) – NMR samples of TIA-1 RRM3 were prepared in 90% H_2O / 10% D_2O solutions of 20 mM potassium phosphate buffer, 50 mM KCl (pH 7.0) at concentrations in a range 0.05-1 mM. NMR spectra were recorded at 25 ºC on 800MHz Varian INOVA and 500MHz Bruker Avance III spectrometers. The Bruker spectrometer was equipped with cryoprobe technology. The spectra recorded in Varian spectrometer were processed with nmrPipe software (21) to be further analyzed with the CcpNmr program suite (22). Those spectra recorded in Bruker spectrometer were processed using TopSpin 3.0 and analyzed with SPARKY (23).

Standard 3D NMR experiments (HNCACB, HNCA and HNCO) were used to assign backbone resonances of RRM3 domain. The coverage of the backbone assignment was 98%. The assigned chemical shifts were deposited at the BMRB with the accession number 18829 and were used to generate the protein 3D structure at CS23D2.0 web server (24). The pdb file generated with NMR chemical-shifts assignments for the 3D structure was used for

data discussion and to build Figures 1, 4, 6 and 7.

The pH effects on TIA1 RRM2 and RRM3 domains were followed by recording ^{15}N-HSQC spectra on 700MHz Bruker Avance III and 800MHz Varian INOVA during titrations of a 0.01 mM sample of ^{15}N-labeled RRM2 domain and a 0.05 mM sample of ^{15}N-labeled RRM3 domain, respectively, in 20 mM potassium phosphate buffer, 50 mM KCl (pH 3.8 for RRM2 and 5.0 for RRM3) with small aliquots of 0.1 M NaOH to gradually increase the pH.

RNA binding of TIA-1 RRM3 was monitored by acquiring ^{15}N-HSQC spectra along titrations of the 5´-AUUUA-3´ RNA oligonucleotide into a sample of 25 μM ^{15}N-labeled RRM3 in 20 mM potassium phosphate buffer, 50 mM KCl, at both pH 5.5 and 7.5 values. The pH value of the sample was verified after each titration step. Weighted average values of ^{15}N and ^{1}H chemical-shift perturbations ($\Delta\delta_{avg}$) of each resonance was calculated as follows: $\Delta\delta_{avg} = (([\Delta\delta_H]^2 + [\Delta\delta_N/5]^2)/ 2)^{1/2}$, being $\Delta\delta_H$ and $\Delta\delta_N$ chemical-shift increments of ^{1}H and ^{15}N, respectively. The threshold value, used to consider significant chemical-shift perturbations from the titration data, was defined as the average of $\Delta\delta_{avg}$ values plus 2 standard deviations ($2S_{n-1}$).

The pH effect on RNA structure was controlled by registering 1D NMR spectra on a 700MHz Bruker Avance III spectrometer at the pH values of 5.5 and 7.5. Samples contained 50 μM of the 24-mer AU oligo 5'AUUUAUUUAUUUAUUUAUUUAUUU 3' and were resuspended in the buffer described before using either 90% H_2O:10% D_20 or 100% D_2O as solvents. The comparison of spectra at different pH values (data not shown) revealed no significant changes in linewidth or chemical-shift perturbations.

pH Titration Curves – Titration curves were obtained by plotting the change in chemical shift as a function of pH for all of the detectable backbone amide protons (δ ^{1}H) and nitrogens (δ ^{15}N) of TIA-1 RRM3. Data from 12 out of 18 affected residues were fitted to a sigmoidal curve model describing a single protonation event with an associated pK_a value: $\delta = (K_a\ \delta_H + [H^+]\ \delta_L)/ (K_a + [H^+])$ where δ_H and δ_L are the chemical-shift values at high and low pH. Fits were obtained in Origin (OriginLab, Northampton, MA) 8.0 by non-linear least squares fitting on the proposed model. The pK_a value was the average of two independent pH titrations with estimated errors of ±10%. The threshold value, used to identify significant perturbations when data from the titrations were analyzed together, was defined as the averaged chemical-shift perturbations ($\Delta\delta_{avg}$) for the system plus 2 standard deviations ($2S_{n-1}$). The reported pK_a values of TIA-1 RRM2 histidines were calculated as in the case of RRM3. ^{15}N-HSQC spectra were assigned according to the work of Kuwasako and collaborators (17) (PDB code 2RNE and BMRB accession number 11376).

Circular Dichroism Spectroscopy (CD) – All CD spectra were recorded on a Jasco J-815 spectropolarimeter equipped with a peltier temperature-control system. RRM3, RRM23 and the RNA oligo samples were in 20 mM potassium phosphate buffer, 50 mM KCl, at both pH 5.5 and 7.5 values. Each spectrum was an average of 20 scans.

The secondary structure analysis of RRM3 was performed recording far-ultraviolet (far-UV) CD spectra (190-250 nm) of 3 μM samples at 25 ºC. RNA binding was monitoring in the UV range (240-330 nm) by adding increasing amounts of TIA-1 RRM23 construct to 3 μM of the 24-mer oligo 5'AUUUAUUUAUUUAUUUAUUUAUUU 3'. A temperature of 10 ºC was chosen to optimize the signal change upon protein binding. The integral of the CD signal between 255 and 265 nm was plotted against the ratio [RRM23]/ [24-mer AU RNA] and fitted to a 1:1 binding site model, as reported before (25).

Fluorescence measurements – Emission spectra were recorded in the range 290-500 nm with an excitation wavelength at 282 nm on a Perkin-Elmer LS-5 fluorimeter equipped with a water-thermostat cell holder at 25 ºC. 10 μM RRM3 samples were prepared in 20 mM potassium phosphate buffer, 50 mM KCl, at the pH values of 5.5 and 7.5. The slits wavelength was 5 nm for both excitation and emission and the path length of the cell was 1 cm. The background signal from the buffer was subtracted.

RESULTS AND DISCUSSION

The pH effect on TIA-1 RRM3 domain – pH NMR titration of TIA-1 RRM3,

over the range of pH 5 – pH 8, showed remarkable chemical-shift differences in superimposed ^{15}N HSQC spectra at high and low pH values (Figure 2). A set of signals corresponding to 18 residues were changing upon increasing pH. Other residues underwent negligible chemical-shift changes since they were insensitive to pH effects. A single resonance was observed for each amide over the tested pH range suggesting that the protonation and deprotonation of side chains is fast on the NMR time scale. Different sigmoidal curves were obtained for perturbed residues with titration data (Figure 3) but most of them could be fitted (see Experimental Procedures) to single pK_a values for both ^{1}H and ^{15}N dimensions. As shown in Table 1, pK_a values were in the range from 6.3 to 6.9.

The averaged chemical-shift perturbations ($\Delta\delta_{avg}$) at high (pH 7.5) and low (pH 5) pH values (see Experimental Procedures) gives an evidence of sensitivity of a particular nucleus to a protonation event. The largest values for backbone amides were observed for the His266 (numbering according to the full length TIA-1 protein, Figure 4A). 18 perturbed amides showed significant perturbations ($\Delta\delta_{avg} > 0.05$ ppm) mainly distributed along four regions of RRM3. Two sequential stretches at N-terminus involved, on one side, Asp192, Glu193 and, on the other, the Val210-Thr215 stretch except for the Leu214. The C-terminus residue slot included Ser250, His253, Val256 and those from Thr262 to Lys269. Residues that overcome the threshold of 0.05 ppm in $\Delta\delta_{avg}$ have been mapped onto the TIA-1 RRM3 backbone (Figure 4B and 4C). As it was expected, strongest effects were found for the three solvent-exposed histidines 248, 253 and 266. In fact, the His248 chemical-shift perturbation could not be determined due to signal broadening beyond the detection limit at pH 7, which is a clear evidence of a pH-dependent changes. Other residues surrounding the three histidines were also perturbed as in the case of Thr211 that is in close proximity to His266.

To check that the structure of RRM3 remains unaltered upon pH, far-UV CD spectra and fluorescence emission measurements of the single tryptophan of this domain (Trp272) have been registered (Figure 5). No substantial changes appear in the CD spectra, indicating that the secondary structure of RRM3 is not affected by the pH. On the other hand, the fluorescence maximum appears at ca. 330 nm at both pH values, which corresponds to a partially buried Trp272 residue. The absence of red-shifted fluorescence (ca. 350 nm) shows no substantial conformational changes or protein unfolding.

The pH effect on RNA binding of TIA-1 RRM3 domain – To assess the effect of pH on RNA recognition by TIA-1 RRM3 domain, its interaction with a short 5-mer AU-rich RNA oligonucleotide, namely 5′-AUUUA-3′, was studied. Since the pK_a values for histidine-protonation events were ca. 7 (Table 1), NMR experiments were carried out at low (5.5) and high (7.5) pH values. Averaged chemical-shift perturbations inferred from the titration of ^{15}N-labeled RRM3 with 5′-AUUUA-3′ revealed not only that RRM3 binds RNA using the canonical platform, which comprises aromatic residues mainly localized at three out of four strands from β-sheet, but also that it occurs at both pH values. Due to the small calculated $\Delta\delta_{avg}$, suggesting a moderate affinity of RRM3 for the tested oligo, the dissociation constant could not be obtained. However striking differences arise from data comparison at tested pH values (Figure 6). Upper panels of Figures 6A and 6B show a detail of the superimposed ^{15}N HSQC spectra along titrations for the same residue revealing chemical-shift perturbations that suggest stronger binding at pH 5.5 than at pH 7.5. These differences were observed for all perturbed residues. Middle and lower panels show the mapping of significantly RRM3 shifted residues ($\Delta\delta_{avg} \geq 0.025$ ppm) upon RNA binding over the backbone and surface representations.

At pH 5.5 titration (Figure 6A), residues undergoing the largest shifts were located at the stretches Tyr206–Gly208 and Lys238–Tyr240, along with Val243, as part of the central β strands (β_1 and β_3). In addition, the set of residues Lys269–Lys274 from β_4 was also involved in RNA recognition. Note that Phe242 resonance overlapped with that corresponding to Gln221, so the $\Delta\delta_{avg}$ values could not be accurately calculated although significant line broadening was observed. Moreover, the

easily-assigned N^{ε} of the indole ring from Trp272 experienced large chemical-shift perturbations, even though its amide signal could not be identified. The titration at pH 7.5 (Figure 6B), in its turn, showed almost the same perturbed residues of RRM3 domain but with significant differences: Tyr206 and Phe242 amide resonances were neither shifted nor broadened. Indeed, the perturbation level of highly affected residues at pH 5.5 (Figure 6A, $\Delta\delta_{avg} > 0.050$) is lower at pH 7.5 (Figure 6B, $0.025 \leq \Delta\delta_{avg} \leq 0.050$) – with the exception of Tyr271 –, as a result of weaker binding affinity between TIA-1 and AU-rich RNA at the last pH value.

A deep analysis of RNA-TIA-1 RRM3 binding event (Figure 6) revealed that aromatic residues from β_1 and β_3 strands – namely Tyr206, Tyr240 and Phe242 – constituted the usual RNA docking platform in most RRMs. In addition, Tyr271 and Trp272 (at least its indole amide) from the end of β_4, along with the motif formed by Gly273 and Lys274 at the C-terminal region, were also involved in RNA interaction. Indeed, the C-terminal stretch Gly273-Lys274, which is well-conserved among TIA-1 analogues, has been previously described to be involved in RNA recognition for Pub1p C-terminal domain (20, Figure 1C). Moreover, it is also taking part in forming hydrogen bonds with RNA in other RRMs type- like PTB family, even though the C-terminal stretch differs from the above (26,27).

Trp272 is part of a pocket where His248 from $\alpha 3$ and Gln197 from $\alpha 1$ are in close proximity (Figure 4C). Hence, the His248-Trp272 interaction may pack the extra N-terminal $\alpha 1$-helix on the RRM3 domain (19,20). Within this interaction network, protonation / deprotonation events of His248 could hinder the anchorage of Trp272 by disrupting cation-pi contacts, thus affecting the RNA recognition platform of TIA-RRM3, as suggested by the intrinsic tryptophan residue fluorescence (Figure 5). In fact, the chemical-shift perturbation experienced by Trp272 N^{ε} nucleus of the indole ring is substantially larger at acidic pH (Figure 6). As a consequence of protonation / deprotonation of TIA-1 RRM3 histidine residues, electrostatic potential (EP) surfaces change at both pH values (Figure 7), especially those protein regions surrounding histidines. EP changes around His248 environment can explain differences on RNA binding affinity of TIA-1 RRM3 due to pH variations. Thus, the disruption of the RNA recognition platform can explain the lower binding of the TIA-1 RRM3 motif at pH 7.5.

The pH effect on the TIA-1 binding to RNA – The assays performed by NMR (Figure 6) with the RRM3 domain to evaluate its interaction with RNA showed too small chemical-shift perturbations to be used for quantitative assessment of binding affinities. To overcome this issue, an additional binding experiment was performed to quantify the pH dependence effect and evaluate whether the overall TIA-1 binding to RNA is significantly affected. A construct that comprises RRM2 and RRM3 domains (TIA-1 RRM23) was used, which is, actually, the responsible unit in TIA-1 / RNA recognition (15). As RRM2 domain contains two histidines (His94 and His96) (17) the pK_a values of their –NH groups values were first checked by NMR pH titrations (pK_a-His94 ca. 5.3 and pK_a-His96 ca. 5.4, Figure 8). This is in agreement with the pK_a prediction of the imidazole group for the RNA binding His96 in the context of RRM23 (pK_a-His96 $\approx$ 5.1) using the PROPKA3 server (28). Similar pK_a values (pK_a < 5.3) have been measured for –NH resonances of those RRM2 residues surrounding both His94 and His96. Altogether indicates that only the three histidines from RRM3 in RRM23 experience the protonation/deprotonation events at the two pH values (pH 5.5 and pH 7.5) used in RNA binding studies.

Secondly, we have assessed the affinity of TIA-1 RRM23 for the 24-mer AU RNA by CD (Figure 9). The protein binds to RNA stronger at pH 5.5 than at pH 7.5 ($K_D \approx 4.4$ nM and $K_D \approx 58.5$ nM, respectively). Such observations demonstrate that RRM23 binding to RNA is pH dependent and this effect is mainly caused by RRM3 domain since the deprotonation of RRM2 in the context of RRM23 is negligible at both pH values used for RNA binding studies.

As previous studies have described, the three domains of TIA-1 protein contribute to RNA binding with RRM2 and RRM3 modules as the main recognition platforms (16) as it happens in other RBPs, such as the central-domains units of KH-type splicing regulatory protein (KSRP) (29) and the N-terminal of Human antigen R (HuR) RRM

modules (25). Whereas TIA-1 RRM2 dominates the interaction, RRM3 enhances it playing an auxiliary role. The pH influence over exposed histidine residues of RRM3 – at positions 248, 253 and 266 – in protonation / deprotonation events around pH 7 is clear. Notably, they are highly conserved among TIA-1 homologous and, in the particular case of His248, it has remained unchanged even in species as *Arabidopsis thaliana* or *Saccharomyces cerevisiae* along evolution (Figure 1C). These observations are well-correlated with RNA binding, which decreases at pH 7.5, leading to shorten the RNA platform by means of His248 deprotonation. It is tempting to speculate that the canonical folding of RRM3 tunes RNA binding capability of TIA-1 according to small pH changes – around the physiological value –. Even though the RRM3 extra α-helix (α_1) fails in directly binding to RNA oligos, its relative orientation regarding α_3 and β_4 could facilitate stable RNA binding (30). Such a similar effect has been recently reported for the transcription factor EGR1 (early growth response protein 1) in its binding to DNA (31). The His382 is well conserved and modulates protein-DNA binding, acting as a pH-dependent molecular switch. Another well-studied example of molecular switches regarding to enviromental pH is the hemagglutinin fusion peptide of the influenza virus (32,33), responsible for the viral penetration into host cells by membrane fusion. Altogether, this pH-dependent mechanism may interfere with the overall RNA binding of TIA-1 given the auxiliary role of RRM3 domain and the different binding affinities of RRM23 by RNA depending on the pH.

Given that the pH between cell cytoplasm and nucleus ranges from ca. 7.2 to 7.7 (34), the evaluation of pH influence over multidomain DNA/RNA binding proteins that act in both compartments is highly relevant. This is the case of the KH-domain vigilin, whose biological functions are poorly understood (35-37), or the TIA-1 herein studied. Overall, our findings suggest that these little changes around the physiological pH values in such cellular compartments could control the RRM3 domain packing and, eventually, the RNA recognition events by TIA-1.

REFERENCES

1. Kedersha, N., Cho, M.R., Li, W., Yacono, P.W., Chen, S., Gilks, N., Golan, D.E., and Anderson, P. (2000) Dynamic shuttling of TIA-1 accompanies the recruitment of mRNA to mammalian stress granules. *J. Cell Biol.* **151**, 1257-1268.
2. Zhang, T., Delestienne, N., Huez, G., Kruys, V., and Gueydan, C. (2005) Identification of the sequence determinants mediating the nucleo-cytoplasmic shuttling of TIAR and TIA-1 RNA-binding proteins. *J. Cell Sci.* **118**, 5453-5463.
3. Förch, P., Puig, O., Kedersha, N., Martínez, C., Granneman, S., Séraphin, B., Anderson, A., and Valcárcel, J. (2000) The apoptosis-promoting factor TIA-1 is a regulator of alternative pre-mRNA splicing. *Mol. Cell* **6**, 1089-1098.
4. Förch, P., Puig, O., Martínez, C., Séraphin, B., and Valcárcel, J. (2002) The splicing regulator TIA-1 interacts with U1-C to promote U1 snRNP recruitment to 5' splice sites. *EMBO J.* **21**, 6882-6892.
5. Izquierdo, J.M., Majós, N., Bonnal, S., Martínez, C., Castelo, R., Guigó, R., Bilbao, D., and Valcárcel, J. (2005) Regulation of Fas alternative splicing by antagonistic effects of TIA-1 and PTB on exon definition. *Mol. Cell* **19**, 475-484.
6. Suswam, E.A., Li, Y.Y., Mahtani, H., and King, P.H. (2005) Novel DNA-binding properties of the RNA-binding protein TIAR. *Nucleic Acids Res.* **33**, 4507-4518.
7. Piecyk, M., Wax, S., Beck, A.R.P., Kedersha, N., Gupta, M., Maritim, B., Chen, S., Gueydan, C., Kruys, V., Streuli, M., and Anderson, P. (2000) TIA-1 is a translational silencer that selectively regulates the expression of TNF-α. *EMBO J.* **19**, 4154-4163.

8. López de Silanes, I., Galbán, S., Martindale, J.L., Yang, X., Mazan-Mamczarz, K., Indig, F.E., Falco, G., Zhan, M., and Gorospe, M. (2005) Identification and functional outcome of mRNAs associated with RNA-binding protein TIA-1. *Mol. Cell Biol.* **25**, 9520-9531.
9. Kawai, T., Lal, A., Yang, X., Galban, S., Mazan-Mamczarz, K., and Gorospe, M. (2006) Translational control of cytochrome *c* by RNA-binding proteins TIA-1 and HuR. *Mol. Cell Biol.* **26**, 3295-3307.
10. Damgaard, C.K. and Lykke-Andersen, J. (2011) Translational coregulation of 5′TOP mRNAs by TIA-1 and TIAR. *Gene Dev.* **25**, 2057-2068.
11. Avni, D., Shama, S., Loreni, F., and Meyuhas, O. (1994) Vertebrate mRNAs with a 5'-terminal pyrimidine tract are candidates for translational repression in quiescent cells: characterization of the translational cis-regulatory element. *Mol. Cell Biol*. **14**,3822-3833.
12. Hamilton, T.L., Stoneley, M., Spriggs, K.A., and Bushell, M. (2006) TOPs and their regulation. *Biochem. Soc. Trans.* **34**, 12–16.
13. Kedersha, N.L., Gupta, M., Li, W., Miller, I., and Anderson, P. (1999) RNA-binding proteins TIA-1 and TIAR link the phosphorylation of eIF-2α to the assembly of mammalian stress granules. *J. Cell Biol.* **147**, 1431-1442.
14. Anderson, P., and Kedersha, N. (2002) Stressful initiations. *J. Cell Sci.* **115**, 3227-3234.
15. Dember, L.M., Kim, N.D., Liu, K.Q., and Anderson, P. (1996) Individual RNA recognition motifs of TIA-1 and TIAR have different RNA binding specificities. *J. Biol. Chem*. **271**, 2783-2788.
16. Bauer, W.J., Heath, J., Jenkins, J.L., and Kielkopf, C.L. (2012) Three RNA recognition motifs participate in RNA recognition and structural organization by the pro-apoptotic factor TIA-1. *J. Mol. Biol.* **415**, 727-740.
17. Kuwasako, K,, Takahashi, M., Tochio, N., Abe, C., Tsuda, K., Inoue, M., Terada,T., Shirouzu, M., Kobayashi, N., Kigawa, T., Taguchi, S., Tanaka, A., Hayashizaki, Y., Güntert, P., Muto, Y., and Yokoyama, S. (2008) Solution structure of the second RNA recognition motif (RRM) domain of murine T cell intracellular antigen-1 (TIA-1) and its RNA recognition mode. *Biochemistry* **47**, 6437-6450.
18. Kumar, A.O., Swenson, M.C., Benning, M.M., and Kielkopf, C.L. (2008) Structure of the central RNA recognition motif of human TIA-1 at 1.95A resolution. *Biochem. Biophys. Res. Commun*. **367**, 813-819.
19. Aroca, A., Díaz-Quintana, A., and Díaz-Moreno, I. (2011) A structural insight into the C-terminal RNA recognition motifs of T-cell intracellular antigen-1 protein. *FEBS Lett*. **585**, 2958-2964.
20. Santiveri, C.M., Mirassou, Y., Rico-Lastres, P., Martínez-Lumbreras, S., and Pérez-Cañadillas, J.M. (2011) Pub1p C-Terminal RRM domain interacts with Tif4631p through a conserved region neighbouring the Pab1p binding site. PLoS ONE **6**, e24481.
21. Delaglio, F., Grzesiek, S., Vuister, G.W., Zhu, G., Pfeifer, J., and Bax, A. (1995) NMRPipe: a multidimensional spectral processing system based on UNIX pipes. *J. Biomol. NMR* **6**, 277-293.
22. Vranken, W.F., Boucher, W., Stevens, T.J., Fogh, R.H., Pajon, A., Llinas, M., Ulrich, E. L., Markley, J. L., Ionides, J., and Laue, E. D. (2005) The CCPN data model for NMR spectroscopy: development of a software pipeline. *Proteins: Struct., Funct., Bioinf.* **59**, 687-696.
23. Goddard, T.D., and Kneller, D.G. (2006) SPARKY 3. University of California, San Francisco.
24. Wishart, D.S., Arndt, D., Berjanskii, M., Tang, P., Zhou, J., and Lin, G. (2008) CS23D: a web server for rapid protein structure generation using NMR chemical shifts and sequence data. *Nucleic Acids Res.* **36**, W496-W502.
25. Scheiba, R.M., Aroca, A., and Díaz-Moreno, I. (2012) HuR termal stability is dependent on domain binding upon phosphorylation. *Eur. Biophys. J.* **41**, 597-605.
26. Oberstrass, F.C., Auweter, S.D., Erat, M., Hargous, Y., Henning, A., Wenter, P., Reymond, L., Amir-Ahmady, B., Pitsch, S., Black, D. L., and Allain, F. H.-T. (2005)

Structure of PTB bound to RNA: specific binding and implications for splicing regulation. *Science* **309**, 2054-2057.

27. Cléry, A., Blatter, M., and Allain, F.H.T. (2008) RNA recognition motifs: boring? Not quite. *Curr. Opin. Struct. Biol.* **18**, 290-298.
28. Olsson, M.H.M, Sondergard, C.R., Rostkowski, M., Jensen, J.H. (2011) PROPKA3: Consistent treatment of internal and surface residues in empirical pK_a predictions. *J. Chem. Theory Comp.* **7**, 525-537.
29. Díaz-Moreno, I., Hollingworth, D., Kelly, G., Martin, S., García-Mayoral, M., Briata, P., Gherzi, R., and Ramos, A. (2010) Orientation of the central domains of KSRP and its implications for the interaction with the RNA targets. *Nucleic Acids Res.* **38**, 5193-5205.
30. Netter, C., Weber, G., Benecke, H., and Wahl, M.C. (2009) Functional stabilization of an RNA recognition motif by a noncanonical N-terminal expansion. *RNA* **15**, 1305-1313.
31. Mikles, D. C., Bhat, V., Schuchardt, B. J., Deegan, B. J., Seldeen, K. L., McDonald, C. B., and Farooq, A. (2013) pH modulates the binding of early growth response protein 1 transcription factor to DNA. *FEBS J.* **280**, 3669-3684.
32. Doms, R.W., Helenius, A., and White, J. (1985) Membrane fusion activity of the influenza virus hemagglutinin. The low pH-induced conformational change. *J. Biol. Chem.* **260**, 2973-2981.
33. Lorieau, J.L., Louis, J.M., Schwieters, C.D., and Bax, A. (2012) pH-triggered, activated-state conformations of the influenza hemagglutinin fusion peptide revealed by NMR. *Proc. Natl. Acad. Sci. USA*. **109**, 19994-19999.
34. Seksek, O., and Bolard, J. (1996) Nuclear pH gradient in mammalian cells revealed by laser microspectrofluorimetry. *J. Cell Sci.* **109**, 257-262.
35. Kruse, C., Grünweller, A., Notbohm, H., Kügler, S., Purschke, W. G., and Müller, P. K. (1996) Evidence for a novel cytoplasmic tRNA-protein complex containing the KH-multidomain protein vigilin. *Biochem. J.* **320**, 247-252.
36. Kruse, C., Willkomm, D. K., Grünweller, A., Vollbrandt, T., Sommer, S., Busch, S., Pfeiffer, T., Brinkmann, J., Hartmann, R. K., and Müller, P. K. (2000) Export and transport of tRNA are coupled to a multi-protein complex. *Biochem. J.* **346**, 107-115.
37. Vollbrandt, T., Willkomm, D., Stossberg, H., and Kruse, C. (2004) Vigilin is co-localized with 80S ribosomes and binds to the ribosomal complex through its C-terminal domain. *Int. J. Biochem. Cell Biol.* **36**, 1306-1318.
38. Pettersen, E.F., Goddard, T.D., Huang, C.C., Couch, G.S., Greenblatt, D.M., Meng, E.C., and Ferrin, T. E. (2004) UCSF Chimera – a visualization system for exploratory research and analysis. *J. Comput. Chem.* **25**, 1605-1612.
39. Koradi, R., Billeter, M., and Wüthrich K. (1996) MOLMOL: A program for display and analysis of macromolecular structures. *J. Mol. Graphics* **14**, 51-55.

Acknowledgments- The authors wish to thank Dr. P. Anderson (Harvard Medical School, Boston, USA) for kindly provide the plasmid containing the TIA-1 full-length protein and Dr. M. Gorospe (National Institutes of Health, Baltimore, USA) for providing the 24-mer AU RNA oligo. Authors also thank the technical assistance at the NMR services in CITIUS, University of Sevilla and are grateful to Prof. Miguel A. De la Rosa and Dr. Antonio Díaz-Quintana for critical reading of the manuscript.

FOOTNOTES

*This work was supported by the Andalusian Government (P07-CVI-02896 and BIO198). Dr. Aroca was awarded with a FEBS Short-Term fellowship in 2011. The access to the Bio-NMR Research Infrastructure is co-funded under the 7th Framework Programme of the EC (FP7/2007-2013) grant agreement 261863.

[3]The abbreviations used are: adenine/uridine rich elements (AREs); averaged chemical-shift perturbations ($\Delta\delta_{avg}$); circular dichroism (CD); dissociation constant (K_D); DNA/RNA binding protein (D/RBP); electrostatic potential (EP); human antigen R (HuR); KH-type splicing regulatory protein (KSRP); nuclear magnetic resonance (NMR); prion-related domain (PRD); RNA recognition motif (RRM); single-stranded DNA molecules (ssDNA); T-cell intracellular antigen-1 (TIA-1); 5' terminal oligopyrimidine tracts (5'TOP); TIA-1 C-terminal domain like RRM (TRRM); TIA-1 related protein (TIAR); untranslated regions (UTR's).

FIGURE LEGENDS

FIGURE 1. TIA-1 RRM3 domain. A) TIA-1 domain organization and the constructs used in this study. B) Ribbon representation of the RRM3 domain with labeled secondary structure elements. All structure representations in the text were created with Chimera software (38) using the pdb file generated from chemical-shifts assignments (BMRB accession number 18829) at the CS23D2.0 web server (24). C) Sequence alignment of TIA-1 RRM3 domain *(Homo sapiens*) with its homologous proteins of *Mus musculus* (Mm), *Homo sapiens* (Hs), *Saccharomyces cerevisiae* (Sc) and *Arabidopsis thaliana* (At). The secondary structure elements are indicated in the protein sequence along with the three histidines mentioned in this work. Sequences are colored by percent of identity, black (90-100%), dark grey (80%), bright grey (60%) and white (< 50 %).

FIGURE 2. NMR pH titration of TIA-1 RRM3 domain in the range of pH 5 – 8. *Upper* - Overlaid HSQC spectra acquired along the titration where most affected residues are marked. According to the pH, HSQC spectra are colored as follows: pH 5.0, red; pH 5.5, orange; pH 6.0, dark green; pH 6.5, light blue; pH 7.0, purple; pH 7.5, light green and pH 8.0, dark blue. *Lower* - Selected regions from overlaid HSQC spectra showing substantial chemical-shift perturbations of some residues**.**

FIGURE 3. Representative pK_a curves indicating the pH dependence of the chemical shifts of backbone amides of TIA-1 RRM3. Data are fitted to a sigmoidal curve model and describes a single protonation event.

FIGURE 4. Distribution of averaged chemical-shift perturbations for pH-affected backbone amides of TIA-1 RRM3. A) The $\Delta\delta_{avg}$ in ppm of signals are calculated according to the Experimental Procedures at high (pH 7.5) and low (pH 5.0) pH values. The red asterisk (*) stands for the His248 resonance, which is broadened beyond the detection limit. B) Mapping of the $\Delta\delta_{avg}$ on TIA-1 RRM3 ribbon. Each view is rotated 180º around the vertical axis. Residues with $\Delta\delta_{avg} > 0.05$ ppm appear in orange. Residues with $\Delta\delta_{avg}$ below the threshold value are blue while prolines or non-assigned residues are in grey. The three exposed histidines are marked with their side-chain traces in yellow. Note that the $\Delta\delta_{avg}$ of His248 has not been calculated due

to the broadening of this amide signal at pH 7.5 beyond the detection limit, as pointed out by an arrow. C) Detail of the three histidines environment showing the residues located within 3.5Å distance.

FIGURE 5. Negligible effects of pH on the TIA-1 RRM3 structure. A) Far-UV (190-250 nm) CD spectra of RRM3 domain. Solid line stands for the spectrum registered at pH 5.5 while dotted line stands for the one at pH 7.5. B) Fluorescence emission of the RRM3 single tryptophan (Trp272) with the same code as in panel A).

FIGURE 6. Binding of TIA-1 RRM3 to the 5' AUUUA 3' RNA at pH 5.5 (panels A) and pH 7.5 (panels B). *Upper* - Detail of the superimposition of ^{15}N-HSQC recorded during the titration. The spectrum for free protein is cyan, whereas the RNA: protein ratios 1.4:1 and 3:1 are represented in orange and red; respectively. *Middle* - Ribbon representation of TIA-1 RRM3 colored according to the chemical-shift changes undergone by their amide resonances upon RNA binding. Residues with $0.025 \leq \Delta\delta_{avg} \leq 0.050$ ppm appear in orange whereas those with $\Delta\delta_{avg} > 0.050$ are in red. Residues with $\Delta\delta_{avg} < 0.025$ ppm are marked in blue; prolines or non-assigned residues are grey. *Lower* - TIA-1 RRM3 surface with the same orientation and color code as in ribbon representation. The asterisk (*) indicates that Trp272 corresponds to the N^{ε} nucleus in the indole ring.

FIGURE 7. Effect of histidine protonation on the electrostatic potential surfaces of TIA-1 RRM3. A) and B) Electrostatic potential surfaces of TIA-1 RRM3 calculated with its three histidine residues protonated and deprotonated, respectively. The electrostatic potential surfaces were created in Molmol (39) using a color ramp for positive (blue) and negative (red) potentials. Each view is rotated 180º around the vertical axis. Black arrows point out main differences between both representations.

FIGURE 8. pK_a values of TIA-1 RRM2 histidines. pK_a curves indicate the pH dependence of the chemical shifts of backbone amides of His94 and His96. Data are fitted to a sigmoidal curve model and describes a single protonation event.

FIGURE 9. Changes in the CD signal in the 255–265 nm range of the 24-mer AU RNA (5´ AUUUAUUUAUUUAUUUAUUUAUUU 3') spectrum during titration with TIA-1 RRM23 construct at pH 5.5 and pH 7.5. Dissociation constants are also shown in each case.

TABLE 1. pK_a values of TIA-1 RRM3 –NH groups.

Residue	^{15}N pK_a	^{1}H pK_a
Glu193		6.20 ± 0.60
Val210	6.40 ± 0.60	6.40 ± 0.60
Thr211	6.40 ± 0.60	
Ser250	6.70 ± 0.70	
His253	6.90 ± 0.70	
Val256		6.50 ± 0.70
Thr262	6.40 ± 0.60	6.30 ± 0.60
Glu264	6.40 ± 0.60	6.80 ± 0.70
Gly265		6.20 ± 0.60
His266	6.40 ± 0.60	6.40 ± 0.60
Val267	6.30 ± 0.60	6.30 ± 0.60
Lys269		6.50± 0.70

Figure 1

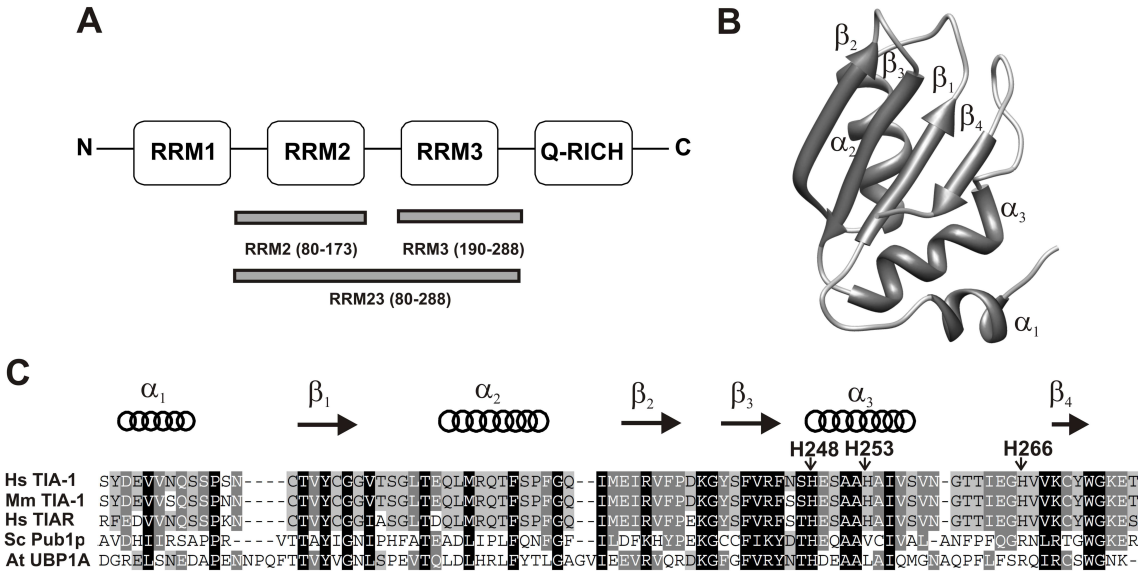
A
N
RRM1
RRM2
RRM3
Q-RICH
C
RRM2 (80-173)
RRM3 (190-288)
RRM23 (80-288)
B
β2
β3
β1
β4
α2
α3
α1
C
α1
β1
α2
β2
β3
α3
β4
H248 H253
H266
Hs TIA-1 SYDEVVNQSSPSN----CTVYCGGVTSGLTEQLMRQTFSPFGQ--IMEIRVFPDKGYSFVRFNSHESAAHAIVSVN-GTTIECHVVKCYWGKET
Mm TIA-1 SYDEVVSQSSPNN----CTVYCGGVTSGLTEQLMRQTFSPFGQ--IMEIRVFPDKGYSFVRFSSHESAAHAIVSVN-GTTIECHVVKCYWGKET
Hs TIAR RFEDVVNQSSPKN----CTVYCGGIASGLTDQLMRQTFSPFGQ--IMEIRVFPEKGYSFVRFSTHESAAHAIVSVN-GTTIECHVVKCYWGKES
Sc Pub1p AVLHIIRSAPPR----VTTAYIGNIPHFATEADLIPLFQNFGF--ILDFKHYPEKCCFIKYDTHEQAAVCIVAL-ANFPFQCRNLRTGWGKER
At UBP1A DGRELSNEDAPENNPQFTTVYVGNLSPEVTQLDLHRLFYTLGAGVIEEVRVQRDKGFGFVRYNTHDEAALAIQMGNAQPFLFSRQIRCSWGNK-

Figure 2

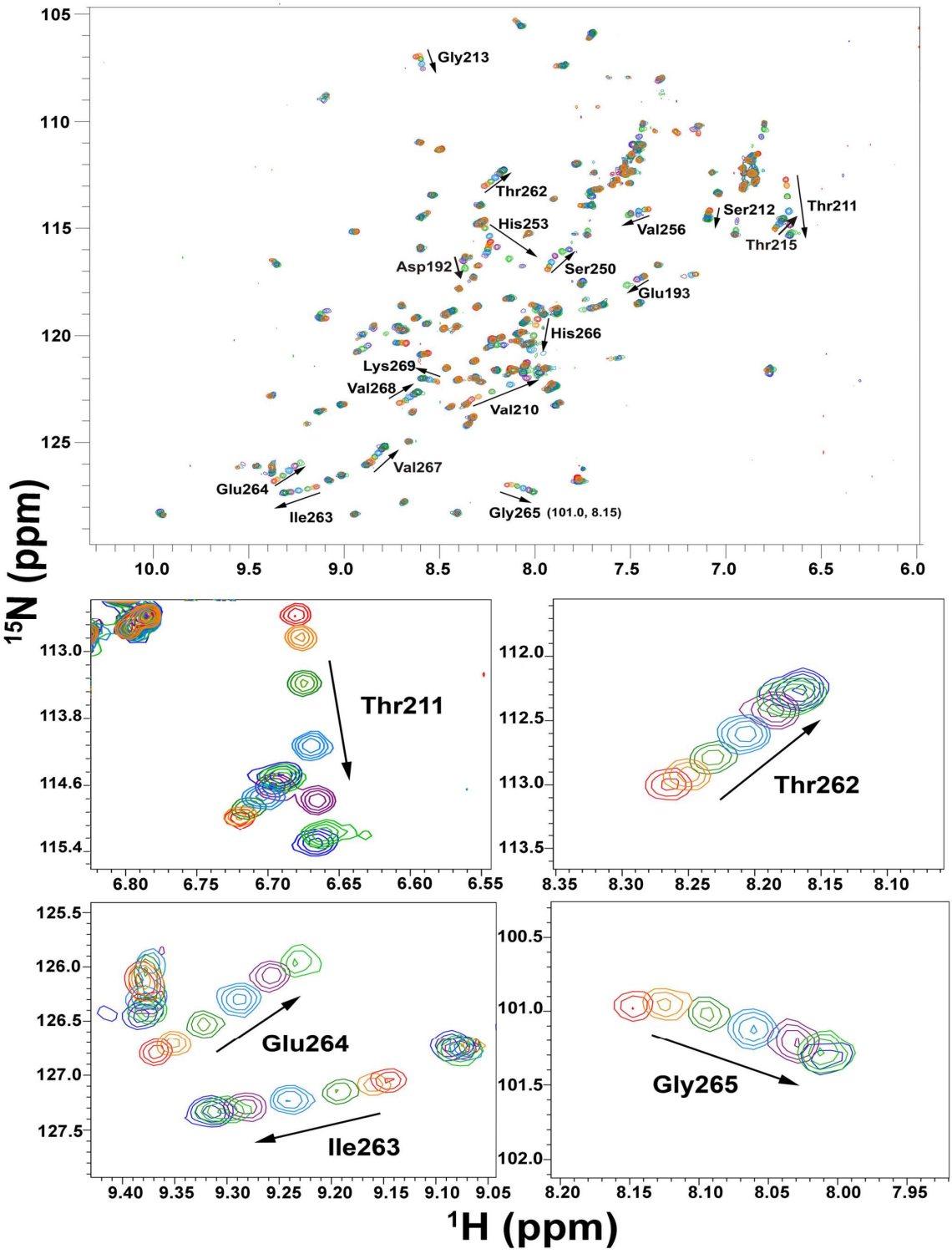
Gly213
Thr262
His253
Asp192
Ser250
Val256
Ser212
Thr211
Thr215
Glu193
His266
Lys269
Val268
Val210
Val267
Glu264
Ile263
Gly265 (101.0, 8.15)
^{15}N (ppm)
Thr211
Thr262
Glu264
Ile263
Gly265
^{1}H (ppm)

Figure 3

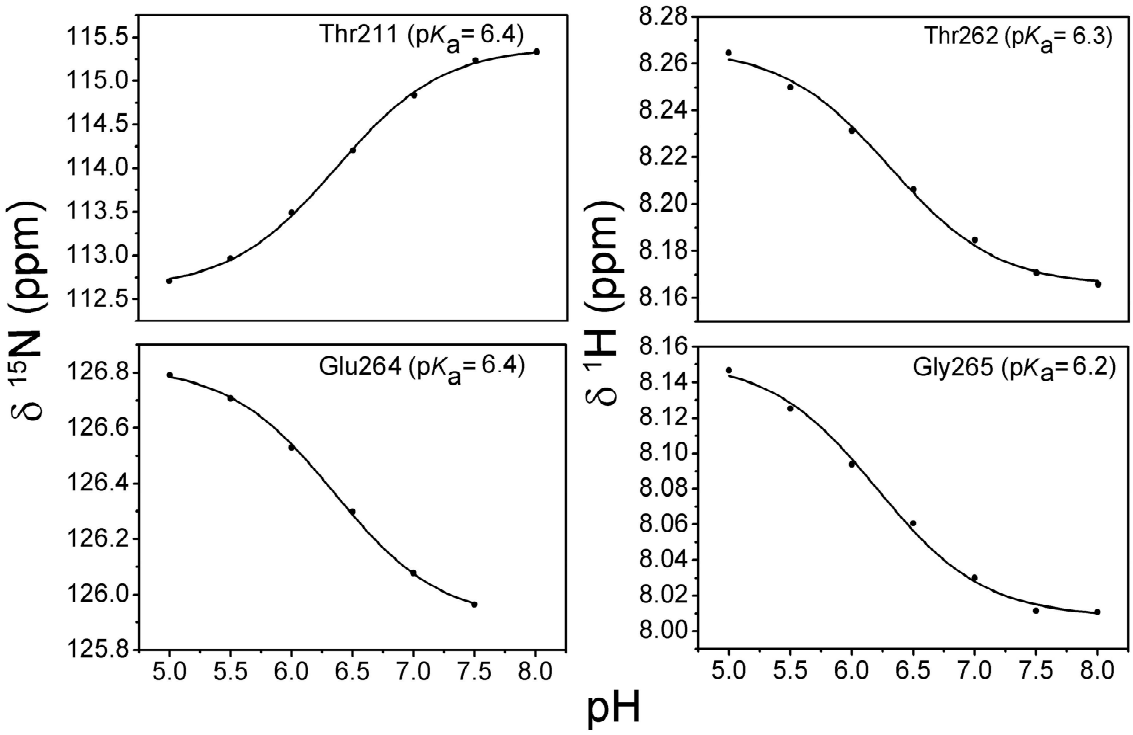
Thr211 (pK_a= 6.4)
Thr262 (pK_a= 6.3)
Glu264 (pK_a= 6.4)
Gly265 (pK_a= 6.2)
δ ^{15}N (ppm)
δ ^{1}H (ppm)
pH
115.5
115.0
114.5
114.0
113.5
113.0
112.5
126.8
126.6
126.4
126.2
126.0
125.8
8.28
8.26
8.24
8.22
8.20
8.18
8.16
8.14
8.12
8.10
8.08
8.06
8.04
8.02
8.00
5.0
5.5
6.0
6.5
7.0
7.5
8.0

Figure 4

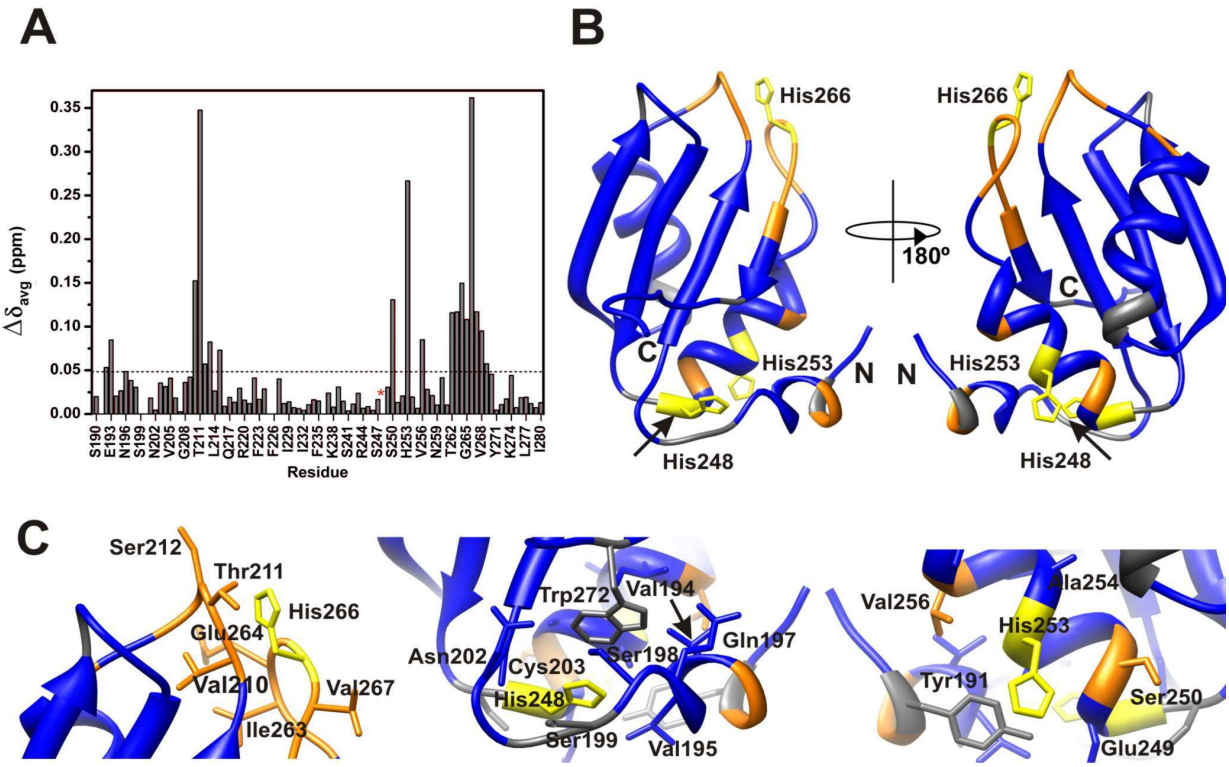
A
B
C
$\Delta\delta_{avg}$ (ppm)
Residue
His266
His253
His248
180°
N
C
Ser212
Thr211
Glu264
Val210
Ile263
Val267
Trp272
Val194
Asn202
Cys203
Ser198
Gln197
Ser199
Val195
Val256
Ala254
Tyr191
Ser250
Glu249

Figure 5

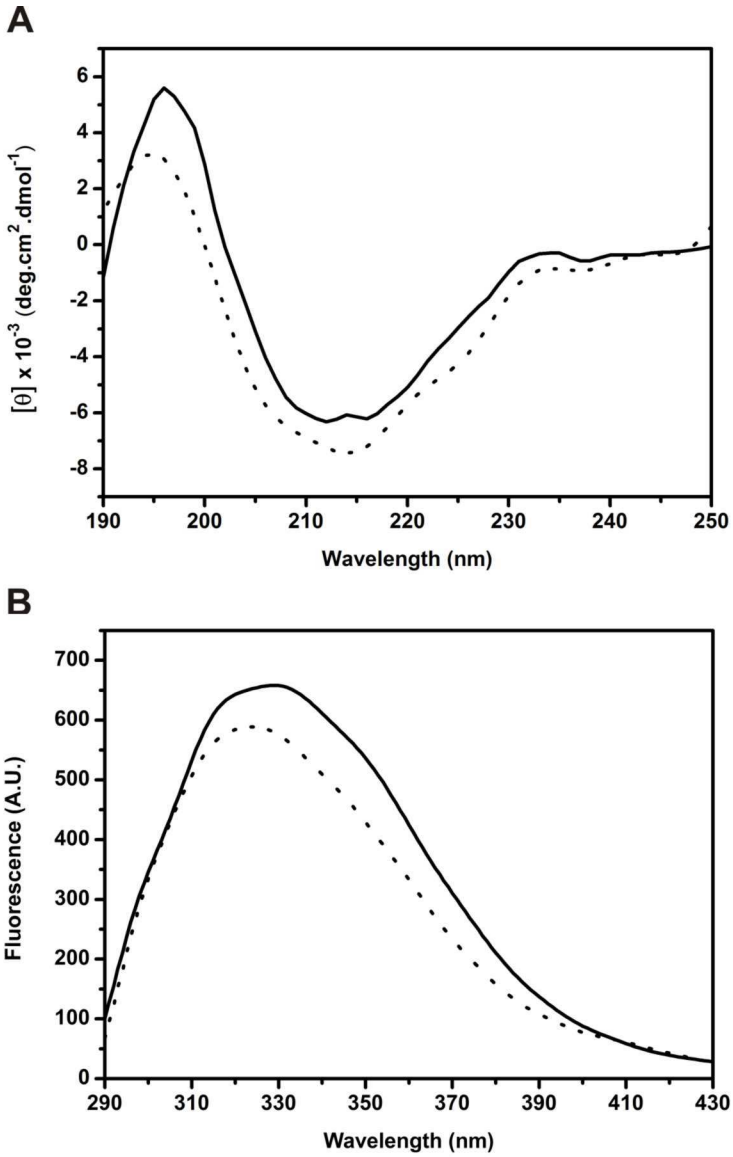
A
[θ] x 10^-3 (deg.cm^2.dmol^-1)
6
4
2
0
-2
-4
-6
-8
190
200
210
220
230
240
250
Wavelength (nm)
B
Fluorescence (A.U.)
700
600
500
400
300
200
100
0
290
310
330
350
370
390
410
430
Wavelength (nm)

a

Figure 6

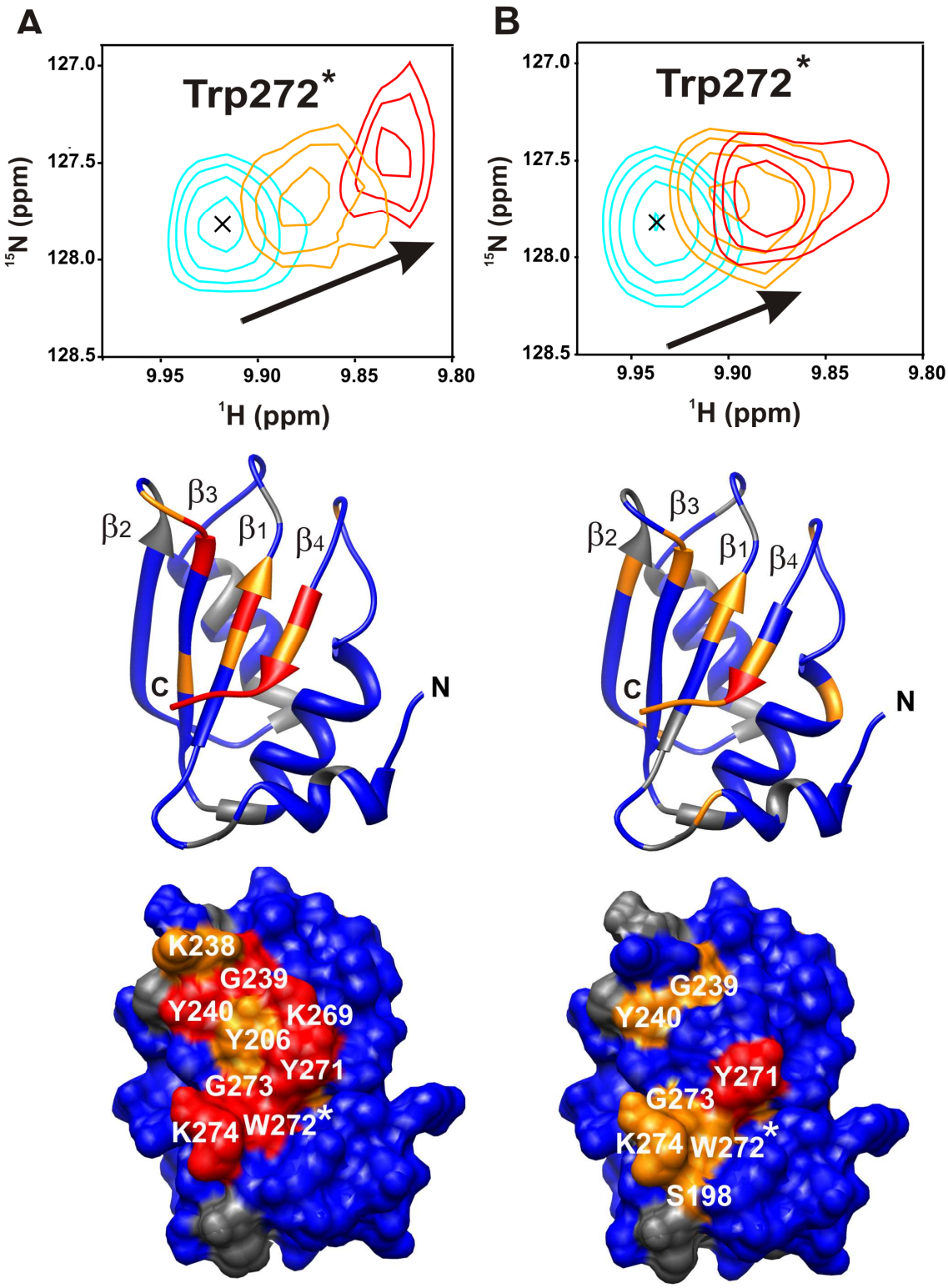
A
B
Trp272*
Trp272*
127.0
127.5
128.0
128.5
^{15}N (ppm)
9.95
9.90
9.85
9.80
^{1}H (ppm)
β2
β3
β1
β4
C
N
K238
G239
Y240
K269
Y206
Y271
G273
K274
W272*
G239
Y240
Y271
G273
K274
W272*
S198

Figure 7

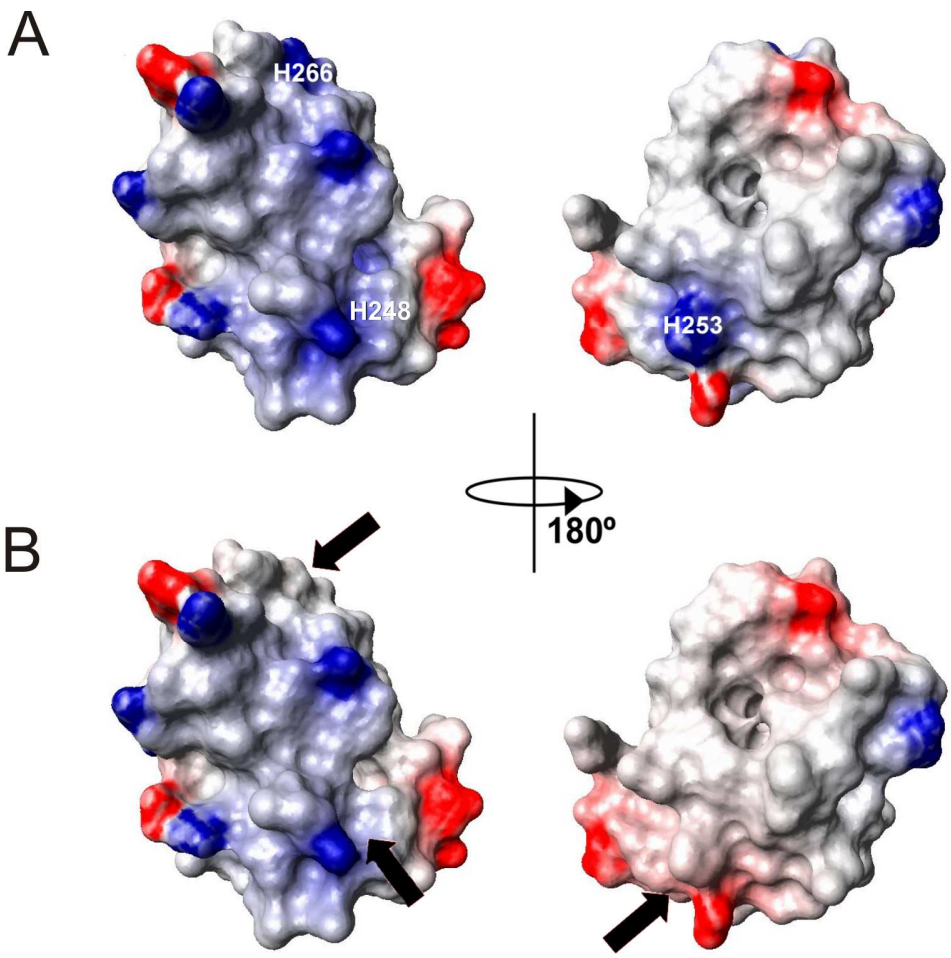

Figure 8

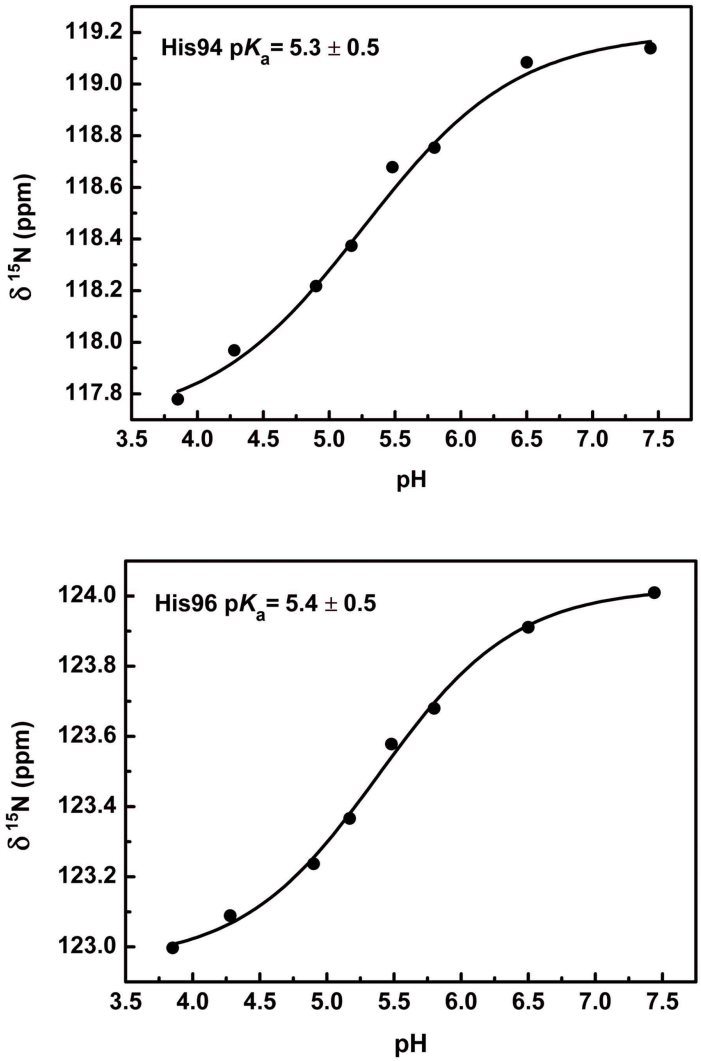
His94 pK_a = 5.3 ± 0.5
δ^{15}N (ppm)
pH
His96 pK_a = 5.4 ± 0.5
δ^{15}N (ppm)
pH

Figure 9

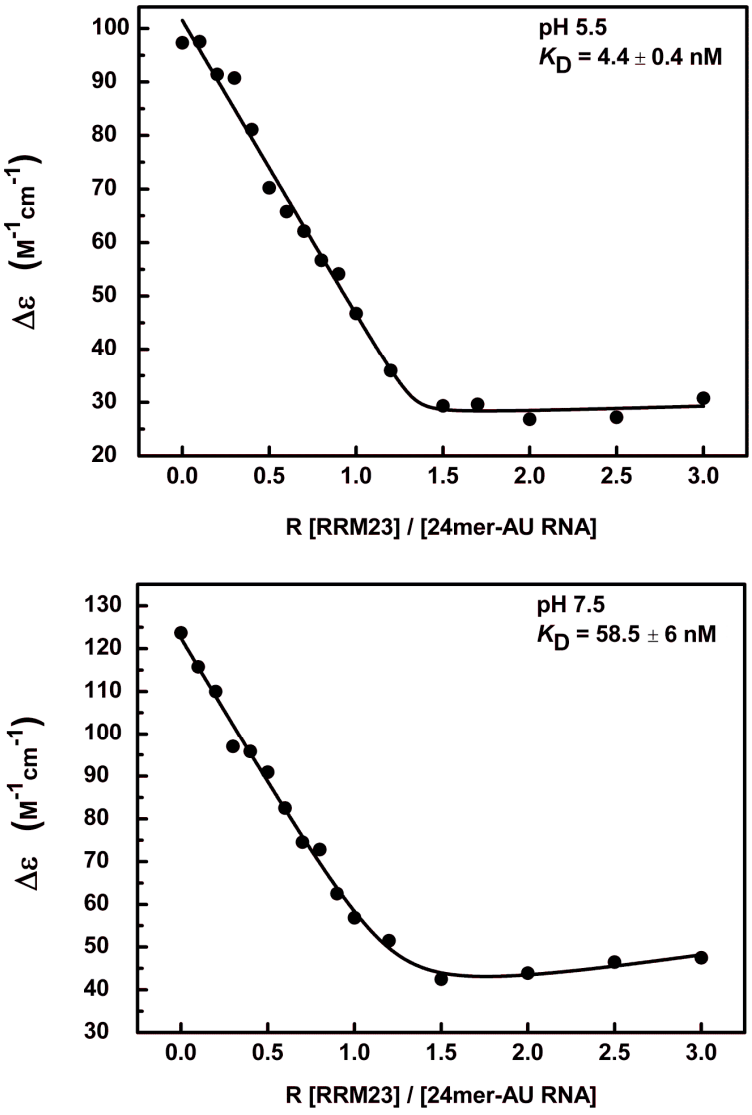
pH 5.5
K_D = 4.4 ± 0.4 nM
Δε (M^{-1}cm^{-1})
R [RRM23] / [24mer-AU RNA]
pH 7.5
K_D = 58.5 ± 6 nM
Δε (M^{-1}cm^{-1})
R [RRM23] / [24mer-AU RNA]